Thermochimica Acta 497 (2010) 77–84

Contents lists available at ScienceDirect

Thermochimica Acta

journal homepage: www.elsevier.com/locate/tca

Thermal desorption of chiral molecules from a nanostructured chiral surface: Insights from computer simulations

Paweł Szabelski [a,*], Tomasz P. Warzocha [a,b], Tomasz Pańczyk [b]

[a] Department of Theoretical Chemistry, Maria-Curie Skłodowska University, Pl. M.C. Skłodowskiej 3, 20-031 Lublin, Poland
[b] Institute of Catalysis and Surface Chemistry, Polish Academy of Sciences, ul. Niezapominajek 8, 30-239 Kraków, Poland

ARTICLE INFO

Article history:
Received 3 July 2009
Received in revised form 21 August 2009
Accepted 25 August 2009
Available online 31 August 2009

Keywords:
Chiral adsorption
Temperature programmed desorption
Monte Carlo simulation
Nanostructured surface

ABSTRACT

Temperature programmed desorption (TPD) of model chiral molecules from a chiral surface with periodic pattern of active sites was studied theoretically using the Monte Carlo method. The simulations were performed for enantiomerically pure and racemic layers adsorbed on the chiral surface with an ordered $(\sqrt{5} \times \sqrt{5})R27^{\circ}$ superstructure of the active sites. It was demonstrated that an efficient separation of the enantiomers on the nanostructured surface could be achieved by suitable manipulating energetic properties of the surface. Moreover, the influence of factors such as lateral interactions in the adsorbed phase and mobility of the adsorbed molecules on the desorption kinetics was examined. The obtained results provided some insights into the mechanism of chiral selection with nanostructured surfaces under ultra high vacuum conditions. In particular, it was demonstrated that effectiveness of the separation decreases with coverage due to reduced chances for the enantiomers to occupy their energetically preferred clusters of adsorption sites.

1. Introduction

Temperature programmed desorption (TPD) is a versatile and robust method to study physico-chemical processes occurring in molecular layers adsorbed on solid surfaces. The main advantage of this technique is that it often provides a clear picture of the interaction pattern of an adsorbate with the surface. Moreover, it also gives the possibility of estimating energetic properties of the surface itself by, for example, resolving the corresponding adsorption energy distribution function (AED) [1,2]. Because of these merits, TPD has become a standard tool in experimental characterization of surface-mediated processes such as catalytic reactions involving simple gases or complex organic molecules, also chiral molecules [3–11]. Valuable information which can be extracted from TPD experiments is the number of types of adsorption sites present on the surface. Moreover, it is often possible to estimate the effect of intermolecular interactions in the adsorbed phase by carrying out TPD experiments at variable coverage. This information is of crucial importance to optimization of heterogeneous catalytic reactions whose products can be largely dependent on the local structure of the adsorbing surface as well as on the interactions between adsorbed molecules. One typical example in this area is stereoselective synthesis of enantiopure substances in the presence of metallic surfaces templated with organic modifiers [12–14]. In this case, the synthesis can be directed towards the target enantiomer by selective preadsorption of appropriate chiral substrates. For instance, it has been demonstrated using TPD that selective adsorption of enantiomers of propylene oxide on a 2-butoxide templated Pd(111) surface occurs only within a narrow interval of the template coverage [4]. A similar tendency has been also observed for Pd(111) surface templated by chiral 2-aminobutanoate species [5].

Temperature programmed desorption has been used recently to examine binding of chiral adsorbates to naturally chiral metallic surfaces [6–10]. An interesting application of this technique has been proposed by Gellman and co-workers who have used TPD to demonstrate the potential of naturally chiral surfaces to differentiate between enantiomers of chiral alcohols [6]. Specifically, the authors have reported the kinetic separation of racemic 3-methylcyclohexanone (3-MCHO) on the chiral Cu(643) surface in which the adsorbed layer becomes richer with one enantiomer due to enantiospecific interaction of the adsorbate with chiral kink sites of Cu(643). It is worth noting that the kinetic separation of racemic 3-MCHO was possible even though the observed difference in the peak desorption temperatures of (R)-3-MCHO on $Cu(643)^R$ and $Cu(643)^S$ was only 3.5 K, that is about 1 kJ/mol difference in desorption energy. To explore further enantiospecific desorption of chiral molecules from naturally chiral surfaces Power et al. have performed MC simulations of thermal desorption of small chiral hydrocarbons from the series of chiral platinum single crystal faces [15]. In this case the largest difference in desorption energy, ~2 kJ/mol, was predicted for the enantiomers of dimethylcyclopropane desorbing from the $Pt(643)^S$ surface. The studies of

* Corresponding author. Tel.: +48 081 537 56 20; fax: +48 081 537 56 85.
E-mail address: szabla@vega.umcs.lublin.pl (P. Szabelski).

0040-6031/$ – see front matter © 2009 Elsevier B.V. All rights reserved.
doi:10.1016/j.tca.2009.08.011

Power have demonstrated the importance of local atomic order which is responsible for the preservation of individual enantiospecific adsorption properties of the surface. In particular, it has been shown using TPD modeling that differences between enantiospecific properties of chiral platinum surfaces are greatly diminished once thermal roughening is considered.

As it follows from both experimental and theoretical studies the key role in selective adsorption of enantiomers on the structured surfaces mentioned above plays local chiral environment of an adsorbed molecule. For those surfaces, it is usually observed that the enantioselectivity results from a one-to-one correspondence in the interaction pattern of the enantiomer with the complementary three-dimensional structure. This structure can be a pocket formed by template molecules adsorbed on a solid substrate or a chiral kink site of a naturally chiral metallic surface. However, as we have demonstrated recently using computer simulations, the one-to-one correspondence which is common for most of chiral adsorbents is not a necessary condition for the selective adsorption of a selected enantiomer [16–20]. Namely, in the approach we adopted previously the enantiodiscrimination was based on the difference between molecular footprints of model enantiomers adsorbing on a solid surface with a special periodic distribution of active sites [16,17]. The obtained results indicated clearly that the preference of the surface for adsorption of one enantiomer under equilibrium conditions could be easily tuned by manipulating structural and energetic properties of the surface [18–20]. In this contribution we continue our investigations and examine whether the chiral nanostructured surface can be further used for an efficient separation of enantiomers carried out under ultra high vacuum.

The main objective of this paper is to explore the possibility of separating enantiomers by their thermal desorption from a surface with active sites forming an ordered chiral superstructure. Additionally, this study aims at understanding of the relation between energetic and structural factors which influence the desorption of chiral molecules from the surface. To achieve this goal we use the MC simulation method to obtain TPD curves of a model chiral adsorbate assuming desorption of both enantiomericaly pure and racemic layers. Moreover, the influence of such factors as intermolecular interactions, surface coverage and relaxation of the adsorbed phase is examined.

2. The model

We consider adsorption of model chiral molecules on a solid surface represented by a square lattice of binding sites with well defined binding energies. The chiral molecules are modeled as rigid S-shaped chain structures composed of four identical segments. A molecular segment can be an atom or a functional group occupying one binding site. In the simplified approach adopted here only that part of the molecule which directly contacts the surface is considered. The remaining part of the molecule which is not involved in the adsorption is disregarded and assumed to be responsible only for preservation of chirality in the bulk phase. According to this assumption, the only important structural property of the molecule is the footprint it leaves on the surface. Fig. 1 shows the chiral footprints of enantiomers S and R consisting of four adsorption sites, each occupied by one segment of the adsorbed enantiomer. The adsorbed enantiomers are prohibited from flipping over and thus from changing their handedness.

The adsorbing surface was built using two types of sites whose strength of interaction with a single segment of the chiral molecule was markedly different. In particular, the energy of interaction between an active site and a segment of the molecule was characterized by ε_a while that between an inert site and the segment

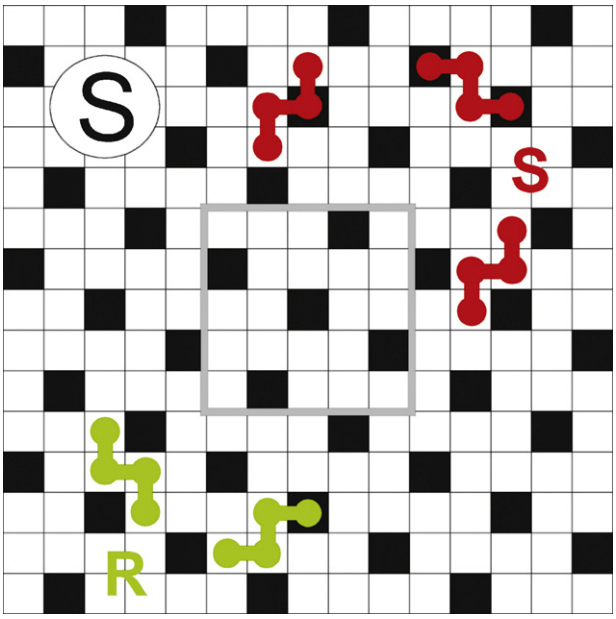

Fig. 1. Schematic view of the S-selective surface with adsorbed enantiomers of type S and R. The thick gray line delimits the unit cell of the surface. The active sites are marked by black squares. Examples of molecular configurations differing by the number of occupied active sites are also shown for each enantiomer.

by ε_i. In order to construct a surface selective towards one of the enantiomers the active sites were distributed on the lattice in such a way that the chosen enantiomer can adsorb more strongly than the other, as assumed in our previous works [16,17]. An example of the distribution meeting this requirement is shown in Fig. 1 for the S-selective surface.

3. Simulation

The simulations were performed on a square $L \times L$ lattice of adsorption sites with $L = 100$. The adsorbing surface consisted of active and inactive sites whose energy of interaction with a single molecular segment was $\varepsilon_a = 20$ kJ/mol and $\varepsilon_i = 10$ kJ/mol, respectively. In the case when intermolecular interactions were allowed in the adsorbed phase we assumed that the segment–segment interactions are fully symmetrical and limited to next neighbors. Accordingly, the energy of interaction between two neighboring segments was characterized by the parameter ω, regardless of the type of interacting molecules (S or R).

The algorithm of thermal desorption was organized as follows [21–24]. In the first step of the simulation the initial temperature was set and the surface was covered with molecules at a fixed amount and composition. The surface coverage was defined as $\theta = 4N/L^2$ where N is the total number of adsorbed molecules. Next, the adsorbed layer was relaxed by a series of attempts to move randomly each adsorbed molecule by one lattice spacing. Relaxation of the adsorbed phase was assumed to be much faster than desorption, so that the equilibrium state was reached each time prior to desorption of the chiral molecules at a given temperature. To that purpose we used a separate relaxation procedure, as it has been done previously by Zgrablich and co-workers [24]. Accordingly, the probability for a molecule to perform a successful jump to the next position was defined as $p_J = \exp[(U_n - U_o)/RT]$, where U_n and U_o are the energies of the molecule in the new and old adsorbed configuration, respectively. These energies were calculated by summing interactions of each molecular segment with the underlying surface and with its neighboring segments. To that end the following

equation was used

$$U = \sum_{j=1}^{4} \varepsilon_j + \omega \sum_{k=1}^{4} \sum_{l=1} s_l \quad (1)$$

where the first sum runs over the lattice sites (a or i) occupied by the molecule and the second sum runs over the next neighbors of each molecular segment which do not belong to the footprint of the molecule. The symbol s_l appearing in Eq. (1) is the occupation number of an adsorption site, being equal 0 or 1, depending whether the site is empty or it is occupied, respectively. To decide if the jump is performed successfully the probability p_J calculated using Eq. (1) was compared with a randomly generated number $r \in \langle 0,1 \rangle$. If p_J was smaller than r the molecule was translated by moving collectively its composite segments by one lattice spacing. Otherwise the trial ended. To equilibrate the system at a fixed temperature we used up to 500 attempts to move each adsorbed molecule.

Once the adsorbed phase has been equilibrated the desorption cycle started. The initial temperature was then increased by a constant value, ΔT. In a single desorption cycle an attempt was made to desorb each molecule with probability

$$p_D = \Delta T \beta^{-1} \nu \exp\left(\frac{-U}{RT}\right) \quad (2)$$

where $\nu = 10^{13}\ s^{-1}$ is the pre-exponential frequency factor and $\beta = 1$ K/s is the heating rate. One important note regarding the assumed value of the pre-exponential factor should be made here. Namely, the model molecules shown in Fig. 1 can be treated as simplified footprints of the corresponding enantiomers of 1,2-dimethylcyclopropane – a small chiral cyclic hydrocarbon for which $\nu = 10^{13}\ s^{-1}$ is a reasonable approximation [15]. However, as shown by Fichthorn and coworkers, the pre-exponential factor can be much greater than $10^{13}\ s^{-1}$ for larger molecules desorbing from solid surfaces [25,26]. This can be the case when the segments of the enantiomers from Fig. 1 are not simple small CH_n groups, being for example aromatic rings etc.

To decide whether the selected molecule is to be desorbed we used a similar criterion as that described for the jump event, that is p_D was compared with r. When all of the adsorbed molecules have been tested the temperature was increased again by ΔT and the whole sequence, including equilibration of the adsorbed phase, was repeated. The MC desorption rate was defined as $\Delta\theta/\Delta T$, where $\Delta\theta$ is the change in the surface coverage induced by increasing the temperature from T to $T + \Delta T$.

The results of the simulations presented in this work are averages over 500 independent starting configurations of the adsorbed enantiomers. For each of these configurations the temperature scan was repeated 200 times and the resulting spectra were subsequently averaged. The values of the energy parameters used in our virtual TPD experiment do not correspond to any real system and they were chosen just to illustrate basic properties of the proposed model.

4. Results and discussion

Before we proceed with thermal desorption of the chiral molecules let us explain origins of enantioselectivity of the surface shown in Fig. 1. To that purpose it is useful to consider possible configurations of each enantiomer (R and S) within a unit cell of the S-selective surface. As it follows from Fig. 1, both enantiomers occupy clusters of four adsorption sites but the maximum number of active sites they can cover is different. For example, for enatiomer S there are three possible configurations in which the molecule occupies: no active sites, one active site and two active sites, as shown in figure. On the other hand, enantiomer R is allowed to adsorb only on clusters containing at most one active site. This

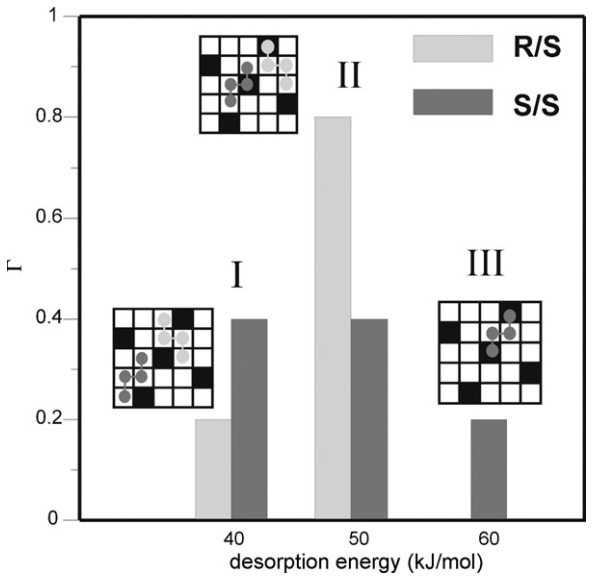

Fig. 2. Energy distribution functions calculated for enantiomers S and R adsorbed on the S-selective surface. The insets show examples of molecular configurations of S and R which correspond to the occupation of a different number of the active sites (black squares), that is: no active sites (I), one active site (II) and two active sites (III).

effect is the key factor which makes the surface from Fig. 1 selective towards enantiomer S. In the following discussion we call the clusters supersites I, II, and III depending whether they are built of 0, 1 and 2 active sites, respectively. Note that the desorption energies associated with supersites I, II and III are equal to $4\varepsilon_i$, $\varepsilon_a + 3\varepsilon_i$ and $2\varepsilon_a + 2\varepsilon_i$, which in our case gives 40, 50 and 60 kJ/mol.

The difference in occupation of supersites I, II and III by the enantiomers can be quantified by calculating adsorption energy distribution functions for R and S. This task involves counting possible configurations of each enantiomer within the unit cell from Fig. 1 which are characterized by the same adsorption energy. The result of this procedure is presented in Fig. 2 together with examples of molecular configurations corresponding to different modes of the normalized distribution functions.

We note that the information provided by Fig. 2 is enough to predict basic features of the TPD spectra obtained for pure enantiomers as well as for their mixture. To illustrate this in Fig. 3 we showed the TPD curves simulated for noninteracting molecules assuming their localized adsorption, that is neglecting relaxation of the adsorbed layer.

As it follows from Fig. 3 the TPD spectra of pure enantiomers R and S consist of two and three distinct peaks, respectively and their shapes agree qualitatively with the shapes of the corresponding distribution functions plotted in Fig. 2. There are three characteristic temperatures at which the molecules desorb intensively from the surface, that is 152.7 K for supersites I, 189.6 K for supersites II and 226.3 K for supersites III, as marked in Fig. 3. These temperatures were calculated using the Redhead formula for first-order desorption. Obviously, only the two first temperatures correspond to desorption of R while for S desorption occurs also at the third temperature. Comparison of the results presented in Figs. 2 and 3 allows to explain relative height and area of the peaks associated with desorption from different supersites. For example, while looking at these figures one can understand why enantiomer R desorbs most intensively at 189.6 K and why the TPD peaks of S at 152.7 K and 189.6 K are of equal area.

Regarding the mixed desorption, the curve corresponding to the racemate (dashed line) is a combination of the TPD spectra obtained for pure enantiomers (solid lines). Namely, the mixed spectrum

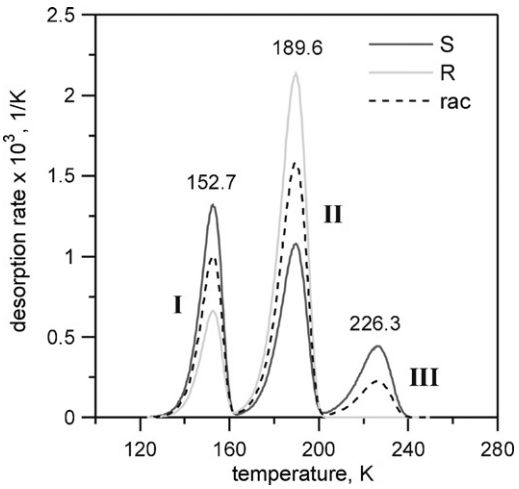

Fig. 3. Thermal desorption curves simulated for pure enantiomers R and S and for their racemic mixture assuming no relaxation of the adsorbed layer; $\theta = 0.16$. The peak temperatures shown in figure correspond to molecular desorption from supersites of type I, II and III shown in Fig. 2.

consist of three peaks of which two first come from desorption of both S and R from sites I and II while the third peak at 226.3 K appears due to desorption of S exclusively. More precisely, the mixed spectrum is just a simple average of the TPD results obtained for pure enatiomers S and R. This can be easily noticed by comparing heights of the corresponding desorption peaks at 152.7 K, 189.6 K and 226.3 K.

We would like to emphasize that the TPD spectra shown in Fig. 3. were simulated to capture essential properties of the desorption kinetics of the enantiomers and they are meant to be a reference which should be helpful in understanding of the behaviour of our system when relaxation of the adsorbed layer and intermolecular interactions are switched on. In fact, the simplified model of desorption enables numerical calculation of the TPD curves from Fig. 3 by solving the associated rate equations. The simulated spectra and their counterparts we obtained numerically (results not shown) agree perfectly.

4.1. Single-component desorption

Let us now focus on a more realistic case in which the adsorbed molecules are allowed to adopt equilibrium configuration on the surface. Fig. 4 presents the TPD curves calculated for the pure enantiomers desorbing from the S-selective surface, for different total initial coverages. As it follows from the top part of Fig. 4, for coverages not exceeding 0.2 the TPD curve simulated for enantiomer R consists of only one peak at 152.7 K which corresponds to desorption from supersites II. When the surface coverage increases beyond ~0.2 the second low-temperature peak at 152.7 K emerges gradually. In this case the molecules of R desorb also from supersites I. The observed changes in the shape of the TPD spectra of enantiomer R can be easily explained by taking into account the result of relaxation of the adsorbed molecules at different surface coverages. Namely, when the density of the adsorbed phase is sufficiently low molecules of R can jump freely and occupy the most energetically favorable supersites II. Additionally this process is enhanced because a single molecule of R has a bigger chance to find supersite II on the surface, compared with supersite I, as it can be clearly seen in the corresponding adsorption energy distribution function plotted in Fig. 2. When the surface coverage increases supersites II saturate quickly and the excess molecules are forced to stay adsorbed on supersites I. In consequence, with increasing surface coverage, the

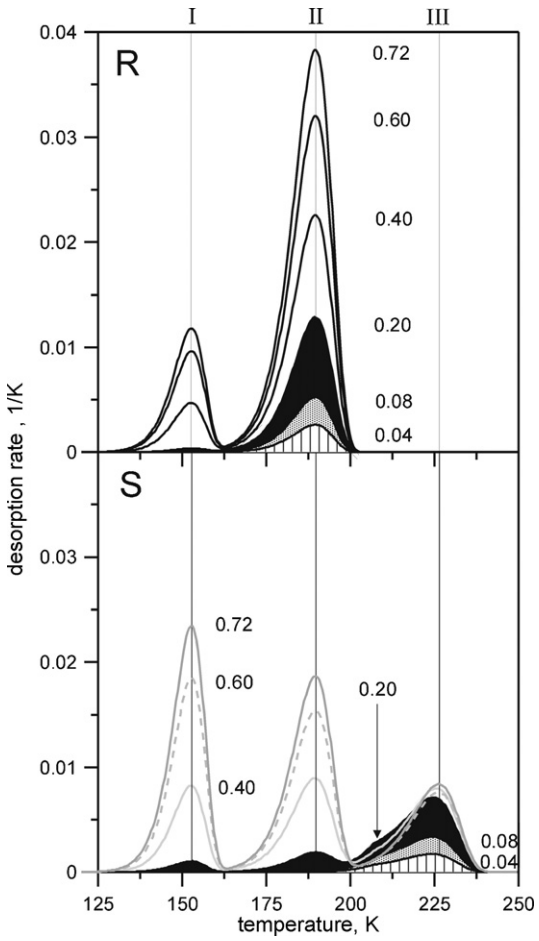

Fig. 4. Thermal desorption spectra simulated for the pure enantiomers, for different total initial coverages indicated in figure. The vertical solid lines correspond to the peak temperatures associated with desorption from supersites I, II and III, these lines are also displayed in the following figures.

TPD curve of enantiomer R becomes similar in shape to the corresponding spectrum obtained for immobile molecules (see Fig. 3). It is worth noting, that the peak temperatures calculated for enantiomer R do not vary with coverage and they are in agreement with the results of Fig. 3.

In the bottom part of Fig. 4 we showed the TPD curves obtained for enantiomer S. In this case, the qualitative effect of surface coverage on the shape of the desorption spectrum is similar to that observed previously for enantiomer R. Specifically, increasing surface coverage causes the low-temperature peaks at 152.7 K and 189.6 K to grow markedly. This effect corresponds to desorption of S from supersites I and II. On the other hand, for low surface coverages (0.04 and 0.08) the molecules of enantiomer S occupy mostly supersites III, that is the most energetically favorable supersites for this enantiomer. Note, however, that the high-temperature peaks obtained for S for coverages 0.04 and 0.08 are broadened towards lower temperatures compared to their counterparts simulated for R (peaks at 189.6 K). Moreover, maxima of these peaks are slightly shifted to lower temperatures. When surface coverage is increased beyond ~0.08 the shape and position of the high-temperature peak of S change apparently. In particular, we can observe a kink on the curve simulated for $\theta = 0.2$ which is indicated by the vertical arrow in the bottom part of Fig. 4. As we will show later this kink appears also at lower coverages but it is much less pronounced.

To explain origins of the observed changes in the shape of the high-temperature peak of enantiomer S let us consider mechanism

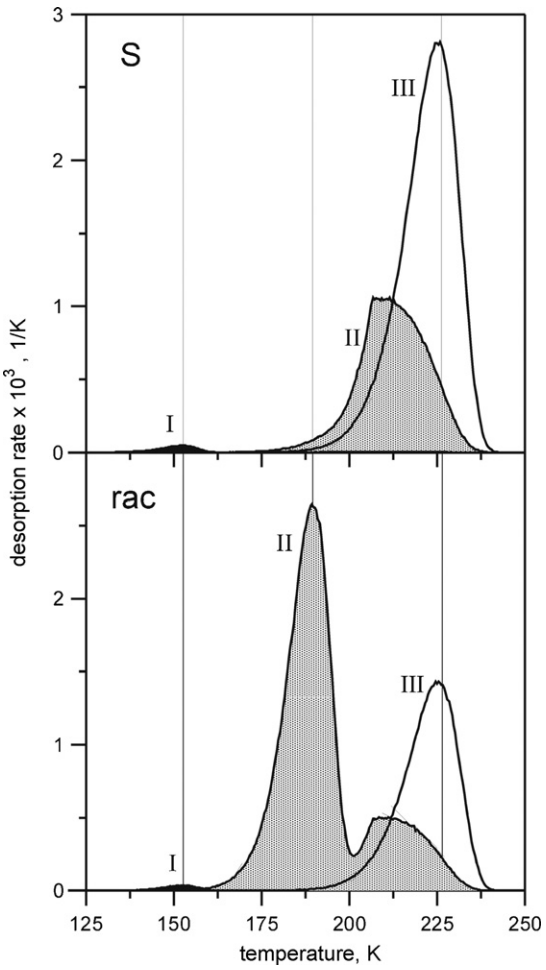

Fig. 5. Composite TPD peaks showing desorption of pure enantiomer S (top) and the racemate (bottom) from supersites I, II and III; $\theta = 0.08$.

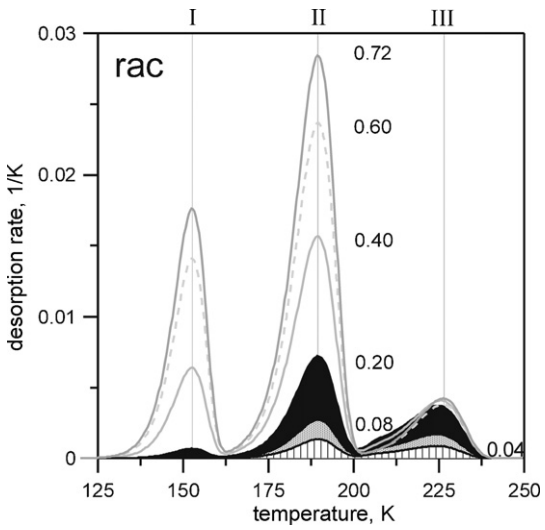

Fig. 6. Thermal desorption spectra simulated for the racemic mixture of enantiomers S and R, for different total initial coverages indicated in figure.

of desorption of this enantiomer from the S-selective surface. To that purpose in the top part of Fig. 5 we plotted the rates of desorption of S from supersites I, II and III simulated for $\theta = 0.08$. The corresponding TPD spectrum shown in Fig. 4 is a sum of the curves plotted in Fig. 5. As it follows from Fig. 5, there are two major contributions to the net desorption rate coming mainly from desorption from supersites II and III. Note, however, that the two contributing peaks are strongly overlapped which leads to significant broadening of the high-temperature peak of S shown in Fig. 4 ($\theta = 0.08$). The main source of this broadening is the substantial shift of the peak of desorption of enantiomer S from supersites II to higher temperatures (the shaded peak). The effect described above is a direct consequence of the relaxation of the adsorbed phase which causes molecules S to jump between supersites II and III. Recall that the probability of a successful jump is controlled by both temperature and difference between energies of adsorption on sites between which the molecule jumps. In our case, the difference between energies of a molecule of S adsorbed on supersites III and II is equal to 10 kJ/mol. Because desorption of S from supersites II starts at relatively high temperatures the probability for a molecule of S to jump from supersite III to supersite II becomes then substantially increased. Moreover, a molecule of S has more freedom in choosing an adsorbed configuration in which it occupies one active site (supersites II) compared to configuration of type III, as seen in Fig. 2 (dark bars II and III). In consequence, the peak of desorption from supersites II shown in the top part of Fig. 5 appears due to enhanced migration of molecules of enantiomer S from supersites III to supersites II and subsequent desorption of these molecules from supersites II.

For temperatures not exceeding about 200 K the rate of desorption from supersites II increases with temperature because of a massive escape of the molecules from supersites III to supersites II during the relaxation step. At this stage the temperature is yet too low to induce fast desorption of enantiomer S from supersites III. When the temperature increases beyond ~200 K the desorption of S from supersites III becomes intense enough to consume large part of the molecules which would be able to jump to supersites II. This change occurs quite rapidly and it gives rise to the kink observed in the TPD spectrum. Note that, the desorption rate from supersites II reaches then a short plateau. This plateau originates mainly form equality between the jump probability of S from supersite III to supersite II in the relaxation step and the probability of direct desorption from supersites III. When the temperature increases further, the chance for desorption from supersites III grows markedly and molecules of S start to desorb directly from these supersites. In consequence the rate of desorption of S via supersites II decreases with growing temperature. At the same time the rate of desorption from supersites III increases markedly and reaches maximum at a temperature which is slightly lower than 226.3 K.

The strong influence of adsorbate relaxation leading to the appearance of the kink on the TPD curves from Figs. 4 and 5 is a special case which does not occur when the energy gap between the energies ε_a and ε_i is large enough or when both these energies are lowered. For example, separate simulations we carried out (results not showed) proved that the kink on the desorption spectrum of S does not appear when $\varepsilon_a = 30$ kJ/mol and $\varepsilon_i = 10$ kJ/mol and when $\varepsilon_a = 15$ kJ/mol and $\varepsilon_i = 5$ kJ/mol. The first set of parameters corresponds to a bigger spacing between peaks I, II and III while usage of the latter causes the entire spectrum shift to lower temperatures.

4.2. Mixed desorption

To examine the possibility of separation of the enantiomers from their racemic mixture we performed simulations whose results are shown in Fig. 6. As it follows from this figure, the mixed desorption spectra of the mobile enantiomers consist of either two or three peaks, depending whether the surface coverage is low or high, respectively. This effect has been observed already for the pure enantiomers and it originates mainly from coverage-dependent

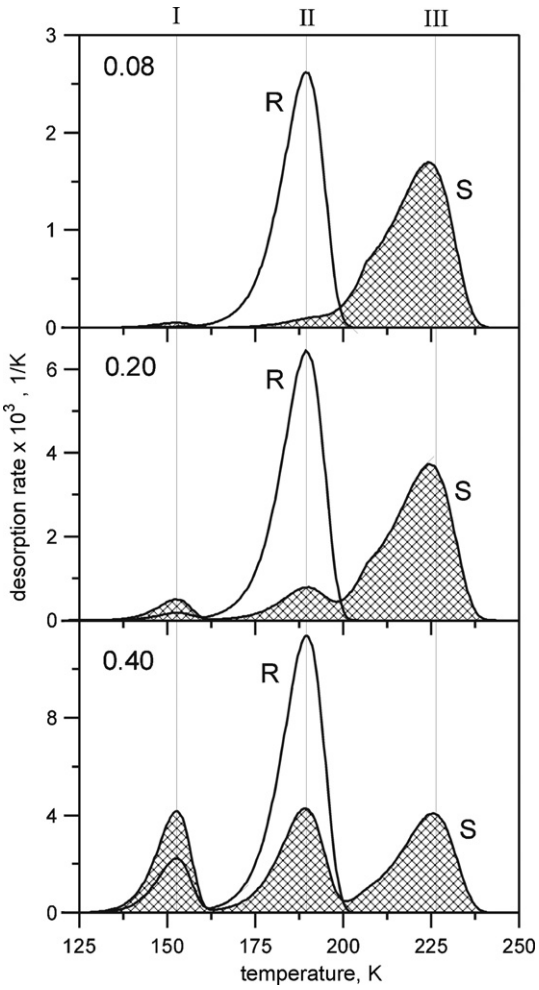

Fig. 7. Deconvoluted TPD spectra of the racemate showing contributions of S and R to the net desorption rate, calculated for the total initial coverages indicated in each panel.

chances of migration of the enantiomers to their energetically favorable supersites II (R) and III (S). As observed before, when the surface coverage increases the possibility for a molecule to make a successful jump to a neighboring supersite drops considerably. Thus, the enantiomers are allowed to occupy their preferred supersites only at low surface coverages. In consequence, for small values of θ we can expect that the peak centered at 189.6 K should be associated with desorption of enantiomer R while the peak at 226.3 K should correspond to desorption of enantiomer S. This situation offers the possibility of separation of the chiral molecules by collecting desorbed fractions containing pure enantiomers. We will return to this problem later in this section.

Note that the mixed spectra from Fig. 6 are quite similar in shape to the TPD curves obtained previously for pure enantiomer S. Obviously, the relative height of the three composite peaks is altered due to interfering desorption of the other enantiomer. An interesting effect is that the kink observed on the TPD spectrum of S appears also in the curve calculated for the racemate. To show this more clearly in the bottom part of Fig. 5 we plotted the rates of desorption of the racemate from supersites II and III. As it follows from Fig. 5, the rate of desorption from supersites II (shaded area) is represented by a two-peaked curve. The first low-temperature peak corresponds to desorption of enantiomer R while the second is associated with desorption of S via superites II, as it has been already observed for this enantiomer in pure layer (compare with the top part of Fig. 5). The origin of the kink in the mixed spectrum

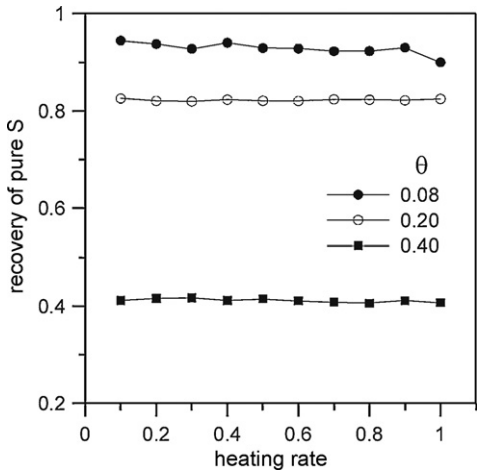

Fig. 8. Influence of the dimensionless heating rate on the recovery of pure enantiomer S from the racemate (see definitions in the text). The results shown in figure correspond to the three systems shown in Fig. 7.

again lies in the relaxation which enables desorption of enantiomer S from supersites III at a lowered temperature. For this reason the kink is transmitted to the mixed spectra and it appears at exactly the same temperature as for pure enantiomer S, that is at about 206.7 K.

Let us now explore the possibility of TPD-based separation of the enantiomers in our model system. This can be easily done by resolving the mixed spectra to obtain individual peaks of desorption of enantiomers R and S. Fig. 7 presents the contributions of R and S to the net rate of desorption from the racemic layer. As it is clearly seen in figure, an efficient separation of the enantiomers is directly possible only at low surface coverages. The efficiency of the separation can be quantified by calculating the area of that part of the high temperature peak of desorption of S which does not overlap with the peak of R centered at 189.6 K. For example, collecting desorbed fractions at $T \geq 202$ K, that is at the temperature at which the desorption rate of R drops to zero, would result in 91%, 78% and 40% recovery of pure S for the coverage equal to 0.08, 0.20 and 0.40, respectively. The term recovery used here means the percentage of the total amount of S that can be obtained in pure form in the TPD experiment. Note that, even though the efficiency of separation drops considerably with coverage we are still able to obtain pure enantiomer S in a single desorption run. In consequence, at higher coverages it is possible to separate fully the enantiomers by performing sequential desorption/adsorption of the R-rich fraction collected below 202 K. For example, separate simulations performed for $\theta = 0.40$ showed that the recovery of pure enatiomer S obtained by this method increases to 76% when one additional run is performed and to 95% when the run is repeated again. Full resolution (recovery >99%) is achieved in the subsequent adsorption/desorption cycle.

Another method to improve resolution of the TPD peaks, apart from lowering the surface coverage can be manipulating the heating rate. Fig. 8 presents the effect of the dimensionless heating rate on the amount of pure enantiomer S which can be obtained from the racemate adsorbed on the S-selective surface at coverage θ. Unfortunately, as it follows from Fig. 8, decreasing the heating rate does not lead to a big change in the recovery of enantiomer S, regardless of the surface coverage. A noticeable effect can be seen only for the lowest value of the coverage ($\theta = 0.08$), for which the recovery increases from 91% to 94% when the heating rate decreases ten times, that is from 1 to 0.1. For the two higher values of coverage the recovery remains nearly constant within the whole range of the heating rate.

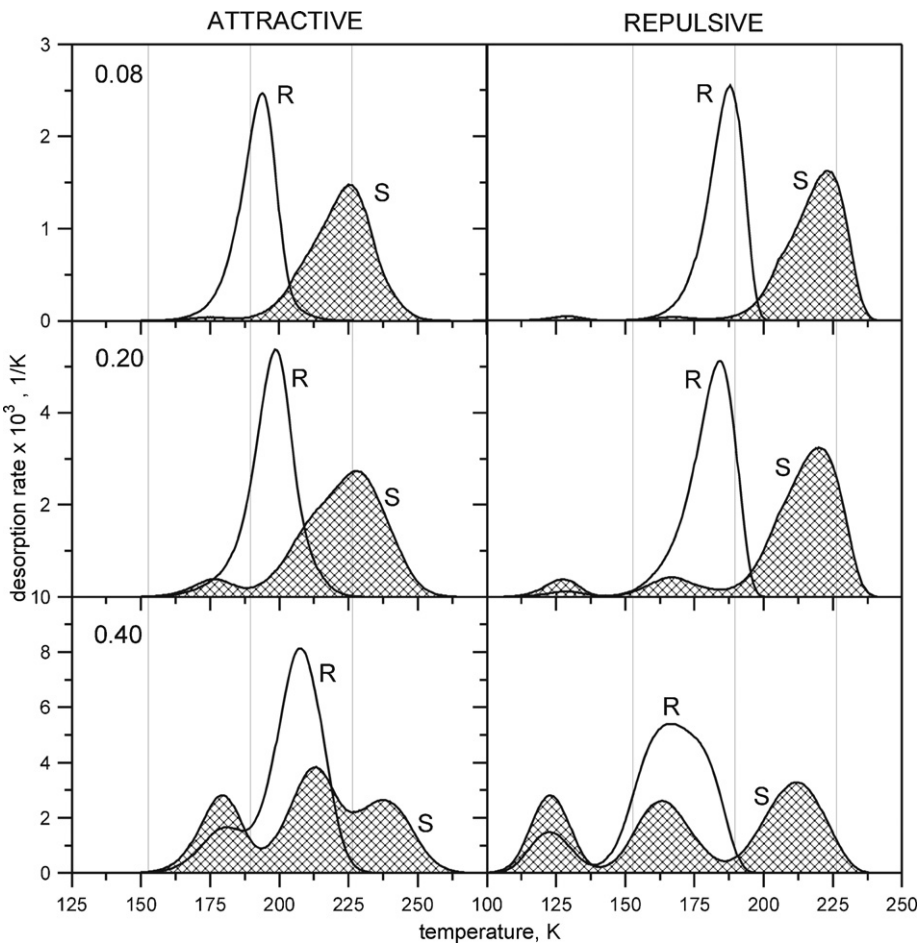

Fig. 9. Influence of lateral interactions on thermal desorption of enantiomers R and S calculated for the racemic mixture, for different total initial coverages indicated in figure. The composite peaks R and S characterize desorption of each enantiomer from the racemic layer adsorbed on the S-selective surface. The segment–segment interaction parameter ω was equal to 1 kJ/mol for attractive interactions and −1 kJ/mol for repulsive interactions.

4.3. *Influence of lateral interactions*

Another factor which can significantly impact the efficiency of separation are interactions between the adsorbed enantiomers. The effect of lateral interactions on the mixed desorption from the S-selective surface is shown in Fig. 9 for different total initial coverages of the racemate. The left part of figure corresponds to $\omega = 1$ kJ/mol (attractions) while the right part shows the results obtained for $\omega = -1$ kJ/mol (repulsions). As it follows from the left part, attractive interactions in the adsorbed layer lead to deterioration of the separation of enantiomers, especially at higher coverages. This can be easily noticed when comparing Figs. 7 and 9. Specifically, attractive interactions are responsible for considerable broadening of the individual peaks of desorption of R and S and thus for their increased overlapping. Note also that the entire spectrum shifts to higher temperatures as the surface coverage increases, which is a direct consequence of an increased net energy of intermolecular interactions at higher adsorbate densities. In consequence the temperature at which the desorption rate of R drops to zero is slightly higher and it equals about 220 K, 226 K and 233 K for the coverage equal to 0.08, 0.20 and 0.40, respectively. When collecting of the S-fraction starts at these temperatures the corresponding recovery of enantiomer S is equal to 59%, 42% and 22%, being almost two times smaller than for the analogous results obtained for the noninteracting enantiomers. In conclusion, the simulations demonstrate that the efficiency of the separation can be decreased substantially even when attractive interactions between adsorbed enantiomers are relatively weak. Note, however, that this tendency does not exclude the possibility of separation of the enantiomers. To achieve full separation of the attracting enantiomers one would require more single adsorption/desorption runs in a cyclic TPD process.

Regarding repulsive interactions, their effect on the separation is much less evident. As it can be seen in the left part of Fig. 9, the extent of overlap between the peaks of S and R at a given coverage is, in general, similar to that observed for the corresponding data obtained for the noninteracting molecules (see Fig. 7). In this case, however, the entire TPD spectrum shifts to lower temperatures with increasing surface coverage and thus the temperature at which the rate of desorption of R diminishes is now equal to about 201 K, 200 K and 198 K for the coverage equal to 0.08, 0.20 and 0.40, respectively. The associated recovery of pure enantiomer S is 91%, 78% and 39% and these values are nearly identical to their counterparts obtained for the noninteracting enantiomers. An interesting feature of the spectrum calculated for $\theta = 0.40$ is the rounded shape of the peak of desorption of R at ~165 K. Note that, in general the shape of this peak does not change significantly with coverage either for interacting or noninteracting enantiomers (compare Figs. 7 and 9), except for the case mentioned just above. A possible explanation of this effect is enhanced repulsion between enantiomers in the dense adsorbed layer, leading to an increased possibility of desorption of R from supersites II, that is from the most densely populated sites by this enantiomer.

5. Conclusions

The results of this study show that the footprint-based chiral selection of enantiomers on the chiral nanostructured surface provides an effective mechanism that can be used in designing chiral separations by temperature programmed desorption. Our investigations showed that the chiral selective surface can be built in a way which is different from those used in fabrication of naturally chiral stepped surfaces or chiraly templated surfaces. For example, the surface can be created by using an exposed surface of a binary alloy crystal whose components form chiral pattern or by using a nanotemplate surface consisting of a well-ordered chiral array of one monolayer deep holes produced by ion sputtering. As we demonstrated, a suitable spatial distribution of the active sites within a unit cell of a flat surface results in preference for stronger binding of the target enantiomer. This effect enables removal of the less retained enantiomer by gradual heating of the adsorbed layer, leaving pure target enantiomer on the surface. The extent to which the less retained enantiomer can be removed from the surface was found to be strongly dependent on both coverage and nature of intermolecular interactions in the adsorbed phase. Specifically, it was shown that the effectiveness of the separation decreases markedly when density of the adsorbed layer grows as well as when attractive interactions between adsorbed molecules are switched on. These negative factors make it difficult to resolve the enantiomers in a single TPD run but they do not exclude the possibility of a complete separation of the enantiomers in a cyclic TPD process. This demonstrates the great potential of the nanostructured chiral surface for applications in continuous chiral separation processes. In particular, this study can be relevant for small and relatively rigid chiral molecules such as chiral, also substituted, hydrocarbons, chiral alcohols and aminoacids and to a wide range of their derivatives.

Acknowledgement

This work was supported by the Polish Ministry of Science and Higher Education grant No. 1 T09A 103 30.

References

[1] T. Pańczyk, W. Gac, M. Pańczyk, A. Dominko, T. Borowiecki, W. Rudzinski, Langmuir 21 (2005) 7311.
[2] T. Pańczyk, W. Gac, M. Pańczyk, T. Borowiecki, W. Rudzinski, Langmuir 22 (2006) 6613.
[3] V. Bustos, D. Linares, A. Gil Rebaza, W.T. Tysoe, D. Stacchiola, L. Burkholder, G. Zgrablich, J. Phys. Chem. C 113 (2009) 3254.
[4] D. Stacchiola, L. Burkholder, W.T. Tysoe, J. Am. Chem. Soc. 124 (2002) 8984.
[5] D. Stacchiola, L. Burkholder, T. Zheng, M. Weinert, W.T. Tysoe, J. Phys. Chem. B 109 (2005) 851.
[6] J.D. Horvath, A. Koritnik, P. Kamakoti, D.S. Sholl, A.J. Gellman, J. Am. Chem. Soc. 126 (2004) 14988.
[7] J.D. Horvath, A.J. Gellman, J. Am. Chem. Soc. 124 (2002) 2384.
[8] J.D. Horvath, A.J. Gellman, J. Am. Chem. Soc. 123 (2001) 7953.
[9] A.J. Gellman, J.D. Horvath, M.T. Buelow, J. Mol. Catal. A 167 (2001) 3.
[10] C.F. McFadden, P.S. Cremer, A.J. Gellman, Langmuir 12 (1996) 2483.
[11] F. Gao, Y. Wang, Z. Li, O. Furlong, W.T. Tysoe, J. Phys. Chem. C 112 (2008) 3362.
[12] R. Raval, CATTECH 5 (2001) 12.
[13] T. Mallat, E. Orlgmeister, A. Baiker, Chem. Rev. 107 (2007) 4863.
[14] D. Rampulla, A.J. Gellman, in: J.A. Schwarz, C.I. Contescu, K. Putyera (Eds.), Dekker Encyclopedia of Nanoscience and Nanotechnology, Marcel Dekker, Inc, New York, 2004, p. 1113.
[15] T.D. Power, A. Asthagiri, D.S. Sholl, Langmuir 18 (2002) 3737.
[16] P. Szabelski, Appl. Surf. Sci. 253 (2007) 5387.
[17] P. Szabelski, D.S. Sholl, J. Chem. Phys. 126 (2007) 144709.
[18] P. Szabelski, D.S. Sholl, J. Phys. Chem. C 111 (2007) 11936.
[19] P. Szabelski, J. Chem. Phys. 128 (2008) 184702.
[20] P. Szabelski, Chem. Eur. J. 14 (2008) 8312.
[21] P. Szabelski, Appl. Surf. Sci. 253 (2007) 5622.
[22] J.L. Sales, G. Zgrablich, Phys. Rev. B 35 (1987) 9520.
[23] J.L. Sales, G. Zgrablich, Surf. Sci. 187 (1987) 1.
[24] J.L. Sales, R.O. Uñac, M.V. Gargiulo, V. Bustos, G. Zgrablich, Langmuir 12 (1996) 95.
[25] K.A. Fichthorn, R.A. Miron, Phys. Rev. Lett. 89 (2002) 196103.
[26] K.E. Becker, M.H. Mignogna, K.A. Fichthorn, Phys. Rev. Lett. 102 (2009) 046101.